

## All-optical production of a large Bose-Einstein condensate in a double compressible crossed dipole trap

Kazuya Yamashita,<sup>\*</sup> Kouhei Hanasaki, Akihiro Ando, Masahiro Takahama, and Toshiya Kinoshita<sup>†</sup>  
*Course of Studies on Material Science, Graduate School of Human and Environmental Studies, Kyoto University,  
 Yoshida-nihonmatsu-cho, Sakyo-ku, Kyoto 606-8501, Japan*

(Received 16 September 2016; revised manuscript received 24 November 2016; published 11 January 2017)

We report on an all-optical production of a  $^{87}\text{Rb}$  Bose-Einstein condensate (BEC) of  $10^6$  atoms. We construct a double compressible crossed dipole trap (DCDT) formed by a high-power multimode fiber laser (MCDT) and a single-mode fiber amplifier (SCDT), which are both operated at  $1.06\ \mu\text{m}$ . A very cold dense gas is first cooled by polarization gradient cooling in a three-dimensional optical lattice. More than  $2 \times 10^7$  atoms are loaded into the enlarged DCDT. Both CDTs are then simultaneously compressed to significantly different sizes followed by evaporation, which is performed by lowering only the MCDT power. The tighter SCDT produces an extremely high collision rate and maintains the trap stiffness, which leads to rapid and efficient evaporation. After 0.4 s, a gas of  $5 \times 10^6$  atoms with a phase-space density of 0.2 is confined within the SCDT alone. Further evaporation in 2.8 s yields a nearly pure BEC of  $1.2 \times 10^6$  atoms in the  $|Fm_F\rangle = |11\rangle$  state. This number is the largest generated among all-optical methods. Our approach significantly improves the atom number of a condensate and circumvents the severe atom loss previously reported for multimode fiber lasers.

DOI: [10.1103/PhysRevA.95.013609](https://doi.org/10.1103/PhysRevA.95.013609)

### I. INTRODUCTION

Since the first realization of a Bose-Einstein condensate (BEC) of an atomic gas, quantum degenerate gases have been important tools for fundamental physics. To create quantum gases, forced evaporation is carried out in a conservative trap at the final stage of cooling [1]. A magnetic trap (MT) and an optical dipole trap (ODT) have been developed. Optical dipole traps have several advantages such as sublevel independence and wide choices of an external magnetic bias field. These features led to realizing a spinor BEC [2], tuning atomic interactions by magnetic fields [3], and creating a molecular BEC [4,5]. Forced evaporation is performed by simply ramping down laser powers [6]. Optical dipole traps initially provide a high phase-space density and a high collision rate [7–9], but power reductions cause the trap confinement to be less. As a result, elastic collision rates and cooling efficiencies are reduced. This is considered one of the negative aspects of ODTs [10].

Recently, to overcome this downside of ODTs, several groups have developed methods such as a magnetically tilted optical trap [11], an ODT with a dimple trap [12,13], or a largely displaced optical trap [14]. In these traps, the depth and confinement are almost independent of laser powers. Even runaway evaporation has been achieved [11,14]. These methods are proven to produce BECs efficiently; however, the condensates are smaller (typically less than or equal to  $2 \times 10^5$ ) than those in MTs [15]. This is mainly because smaller atom numbers are initially loaded into the trap. Tight confinement causes a reduction of a trap volume, which limits the number of atoms recaptured from a precooling stage. This is another downside of ODTs. How to increase initial loading

numbers while maintaining cooling efficiency is a key focus of this field of study.

One approach has been the use of a compressible crossed dipole trap (CDT) demonstrated by Weiss and co-workers [16,17]. In this approach, the preparation of a very cold gas with high phase-space density is the first important step. The gas was then loaded into a shallow but large-volume CDT and dynamically compressed. A nearly pure BEC of  $3.5 \times 10^5$   $^{87}\text{Rb}$  atoms was produced in a 3.3-s evaporation time [17].

However, the initial number is still limited by the level of the available laser power and there is still some room for improvement. One of the solutions is to use high-power fiber lasers (FLs). Recent advances in fiber laser technology have produced various types of high-power FLs or fiber amplifiers.<sup>1</sup> Multimode FLs are generally inexpensive and more robust than single-mode FLs. On the other hand, it has been pointed out that two longitudinal modes resonantly pump atoms to the upper hyperfine sublevels and the following hyperfine exchange collisions cause severe two-body losses [19–21]. Lauber *et al.* found that the pumping rate depends on the beam intensity and demonstrated the BEC creation by using a rapid evaporation sequence [19]. When applying such multimode FLs to the compression scheme, how to suppress the pumping and how to eliminate the loss become further challenges.

In this paper we present an approach to circumvent these problems and describe an all-optical method to produce a  $^{87}\text{Rb}$  BEC of  $10^6$  atoms in a 3.6-s evaporation time. We construct a double compressible crossed dipole trap (DCDT) consisting of two CDTs with a high-power multimode FL (MCDT) and a single-mode fiber amplifier (SCDT), both operated at  $1.06\ \mu\text{m}$ . We employ polarization gradient cooling in a three-dimensional (3D) optical lattice to produce a very

<sup>\*</sup>yamashita.kazuya.45m@st.kyoto-u.ac.jp

<sup>†</sup>kinoshita.toshiya.6x@kyoto-u.ac.jp;

<http://www.amo.phys.jinkan.kyoto-u.ac.jp/>

<sup>1</sup>Very recently, a BEC with  $1.2 \times 10^6$  spinless  $^{174}\text{Yb}$  atoms was produced in an  $\sim 10$ -s evaporation time by using the time-averaged potential with a 100-W fiber laser. See Ref. [18].

cold gas and load it into the large-volume DCDT supported by a high-power multimode FL. Then the SCDT is minimized, while the MCDT is compressed to a certain intermediate size to avoid severe loss of atoms. The trap stiffness depends only on the tight SCDT and the extremely high elastic collision rate allows us to rapidly lower the MCDT power. We confirm that high evaporation efficiencies are maintained just before the BEC transition. We also show that evaporation during and after the compression significantly accelerates atom loading into the SCDT center [13]. This transfer is completed in 400 ms, much faster than that in any other known combination traps. Further evaporation in the SCDT alone yields a nearly pure BEC of more than  $10^6$  atoms in the  $|Fm_F\rangle = |11\rangle$  state.

This paper is organized as follows. We first describe laser cooling before the initial loading and the setup of the DCDT in Sec. II. In Sec. III we explain the loss in the MCDT and present the idea of a DCDT to circumvent it. The compression sequence and evaporation procedures are presented in Sec. IV. Efficient loading into a tight region of the DCDT is discussed in Sec. V. Finally, we summarize our results in Sec. VI.

## II. EXPERIMENTAL SETUP

### A. Preparation of precooled atoms

A rubidium sample is heated to  $\sim 400$  K in an oven chamber and its vapor is collimated into an atomic beam by using a soda-glass capillary plate. The beam, passing through a differential pumping tube, is slowed down by frequency chirping before entering an ultrahigh-vacuum optical cell. Typically,  $\sim 10^9$  atoms are captured in a standard magneto-optical trap (MOT) in 2.5 s. The atomic beam is then blocked by a mechanical shutter in the oven chamber. The background pressure in the optical cell is less than  $10^{-8}$  Pa during experiments.

The MOT light is generated by an external cavity laser diode (ECLD) seeding tapered amplifier (TA). Its frequency is detuned by  $-20$  MHz with respect to the transition frequency of  $5S_{1/2}F = 2 \rightarrow 5P_{3/2}F' = 3$ . The light is transferred through a single-mode polarization maintaining fiber. At the maximum, 400 mW is available and then divided into three MOT beams and one slower beam. Each MOT beam, with a  $1/e^2$  diameter of 18 mm, is 100 mW and retroreflected. The slower beam is one of the sidebands produced by an electro-optic modulator (EOM). The EOM frequency is scanned over 350 MHz in 7 ms. The repumping beam from another ECLD is retroreflected at the cell. The slower repumping beam is also produced upon traveling through the same EOM.

After the MOT loading, we shut off both slower beams and double the field gradient to transiently compress the MOT (CMOT). At 23 ms later,  $3 \times 10^8$  atoms with a peak density of  $6 \times 10^{11}$  atoms/cm<sup>3</sup> are obtained. At the same time, the magnetic field is turned off and the gas is loaded into a 3D far-off-resonance optical lattice (FORL) for polarization gradient cooling (PGC). Polarization gradient cooling in a 3D FORL works more efficiently than in free space, in particular, for a dense sample [22]. The lattice light is blue detuned by 45 GHz and linearly polarized. Three standing waves have frequency differing by 80 MHz. The beam radii are 600  $\mu$ m. The resulting lattice depth is 330  $\mu$ K and sublevel independent. The 3D FORL is suddenly turned on to 170  $\mu$ K

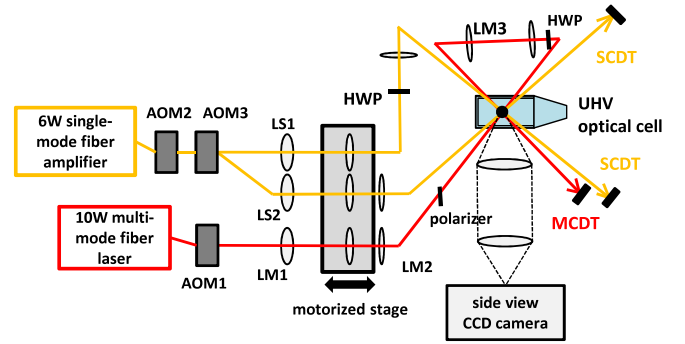


FIG. 1. Schematic configuration of the DCDT. AOM1 and AOM2 control each trap depth and AOM3 creates two separate beams of the SCDT with 80 MHz offset. Three lenses LS1, LS2, and LM1 and their corresponding pairs on a motorized stage form 1:3.3 telescopes, respectively. Here HWP denotes a half waveplate. The side view imaging system is composed of a pair of  $f = 150$  mm achromatic lenses with a 50 mm diameter. The top view imaging system is not shown.

depth and then adiabatically ramped to its full depth in 300  $\mu$ s. For the first 3 ms, PGC is performed by  $-100$ -MHz detuned weak MOT beams and  $-15$ -MHz detuned repumping beams. The final cooling is continued for 9 ms, leaving most of the atoms in the dark states. Under optimized condition, atoms are cooled down to 13  $\mu$ K. The fraction of atoms bound in the vibrational ground state is calculated to be  $\sim 70\%$ . The 3D FORL recaptures 80% of the atoms in the CMOT, while maintaining a high density. The lattice beams are provided by two TAs coupled with one common ECLD. For comparison, we carried out PGC in a 3D FORL created by using a Ti:sapphire ring laser under the same conditions explained above. We obtained virtually the same results. The amplified spontaneous emission from the TA was thus negligible after the optical fiber.

After the PGC, but before turning off the 3D FORL, we optically pump atoms to the  $|Fm_F\rangle = |11\rangle$  state, which is the lowest energy state. A 20-G bias magnetic field with a gradient of 30.7 G/cm is applied. The gravity force is canceled out for  $|11\rangle$  (as well as  $|2-1\rangle$ ), for which we can make a shallow but very large conservative optical trap in the next stage. A near-resonance  $\sigma^+$  polarized beam and two  $\pi$ -polarized depumping beams illuminate the trap. The two depumping beams are red detuned by 50 and 100 MHz from the  $F = 2$  to  $F' = 2$  transition, respectively. More than 90% of the atoms are transferred to the  $|11\rangle$  state in 2 ms. The 3D FORL is then adiabatically turned off in 400  $\mu$ s and completely shut off at a lattice depth of 1.5  $\mu$ K. The atoms are further cooled down to 2.0  $\mu$ K. In the end,  $2.5 \times 10^8$  atoms with a phase-space density (PSD) of  $10^{-3}$  are produced. This is a good starting condition for loading into a shallow optical trap.

### B. Optical setup of a DCDT

First, we describe the setup of a DCDT. A schematic diagram is shown in Fig. 1. A linearly polarized, 10-W

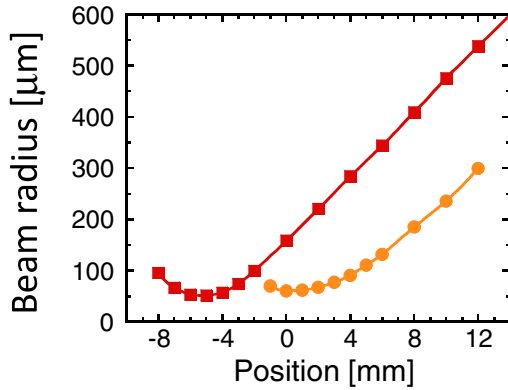


FIG. 2. Transverse beam radii ( $1/e^2$  radii) of the MCDT (red squares) and SCDT (orange circles) at the crossing point as functions of the stage positions. For convenience, the location to minimize the SCDT is defined as zero. The vertical radii have similar dependences, but due to astigmatism, each curve is slightly shifted. The uncertainty of the radius is  $\pm 5\%$ .

multimode fiber laser<sup>2</sup> is operated at 1064 nm. The beam is positioned to pass through a lens mounted on a linear translation stage<sup>3</sup> and to propagate into the optical cell in the horizontal plane. The beam enters the cell twice in a bow-tie geometry, crossing at a nearly right angle. To avoid interference, the two beams are purely linearly polarized and orthogonal to one another. By moving the stage, we are able to control the beam radii, resulting in a compressible crossed dipole trap (MCDT). A 1:1 telescope system is inserted to ensure that both radii are nearly equal at the crossing point. Each beam is focused by a  $f = 500$  mm lens and the Rayleigh length is  $\sim 10$  mm. The first entering beam power  $P_m$  is 8.5 W and the second beam power is 7.7 W.

The SCDT is created by a linearly polarized, 6-W fiber amplifier. The seed laser is a single-mode distributed feedback laser diode<sup>4</sup> operated at 1063 nm. The first acousto-optic modulator (AOM) controls the total power and the second AOM divides the beam into two arms with 80-MHz frequency offset. For the operation to last longer, we limit the amplified power  $P_s$  to less than 2 W/beam. Each beam passes through its own zoom lens at the same linear stage and crosses one another at a right angle. The two beams have nearly the same radius at the trap position throughout the compression. Both the MCDT and the SCDT are simultaneously compressed, but their radii are minimized at a different stage position (Fig. 2). The compression sequence plays a crucial role. We will describe this in Sec. III C.

The spectral width of the multimode FL is less than 0.1 nm and the mode spacing is measured to be approximately 5 MHz. The linewidth of the distributed feedback (DFB) laser diode (LD) is narrowed to be less than 200 kHz by using a reference cavity. All the results presented in this paper were obtained under this condition. However, even at the

free-running operation (short time linewidth  $\sim 2$  MHz, as in the DFB LD's specification data), we did not observe any difference within an experimental uncertainty.

### III. CONSTRUCTION OF A DOUBLE COMPRESSIBLE CDT

#### A. Compressible CDT

A compressible CDT was first demonstrated for Cs atoms [16] and is considered a key technique for an all-optical production of a  $^{87}\text{Rb}$  BEC in Ref. [17]. A PGC-cooled gas is density limited. Thus, a large volume CDT is preferable to recapture the atoms, while keeping the depth larger than the kinetic energy. An initial trap size is determined by a balanced combination of volume and depth. After loading, however, the trap needs to be compressed to enhance an elastic collision rate. Although an adiabatic compression does not change the PSD, it remarkably alters the collision properties. Assuming that evaporation is negligible, the thermodynamic quantities follow simple scaling laws [10,17]. The elastic collision rate  $\Gamma_{\text{col}}$  changes in proportion to a square of the trapping frequency  $\omega^2$ . For an optical trap with a laser power  $P$  and a beam waist  $w$ , the depth  $U \propto Pw^{-2}$  and  $\omega \propto P^{1/2}w^{-2}$ , thus  $\Gamma_{\text{col}} \propto Pw^{-4}$ . These relations clearly indicate that squeezing a trap drastically increases  $\Gamma_{\text{col}}$ .

#### B. Compression of a MCDT

To confirm whether a multimode FL can be applied to the compression scheme or not, we first investigate the atom loss. Atoms were loaded into the MCDT at a radius of  $440 \mu\text{m}$ , which is the initial size used in an actual sequence.<sup>5</sup> The trap was then compressed to different sizes for a duration of 300–450 ms. We confirmed that the cloud center and width never oscillate. The compression is thus adiabatic with respect to atomic motions. Changing the hold time after the compression, we measured the remaining atom numbers and the temperatures. The results are shown in Fig. 3(a). After the initial losses, the atom number continued to decrease with the hold time due to unforced evaporation or heating. The loss of atoms is clearly affected by the beam intensity. For weak intensities, the decay becomes moderate after the initial loss. The following unforced evaporation results in gradual increases of the truncation parameter  $\beta = U_m/k_B T$ , as plotted in Fig. 3(b). At higher intensities greater than or equal to  $25 \text{ kW/cm}^2$  (for one beam), however, the loss never settles down. This cannot be explained by evaporation because the gas is heated for a longer hold time [see Fig. 3(b)]. At very high intensities, the heating outpaces cooling. We did not observe these losses or heating under the same trap conditions when using a single-mode fiber amplifier. This clearly indicates that the severe loss and the heating originate from the multimode FL. Figure 3(c) shows the decay rates for longer hold times. Obviously, the loss rate suddenly changes around the peak intensity of  $20 \text{ kW/cm}^2$  or 8.1 W for a  $150\text{-}\mu\text{m}$  radius. We regard this as the threshold intensity  $I_{th}$ .

<sup>2</sup>ASF15R29, Furukawa Electric Co., Ltd.

<sup>3</sup>GTS150, Newport.

<sup>4</sup>DFB LD, Eagleyard photonics EYP-DFB-1064-00080-1500-TOC03.

<sup>5</sup>The beam radius  $w_r$  represents transverse  $e^{-2}$  radius unless specified otherwise.

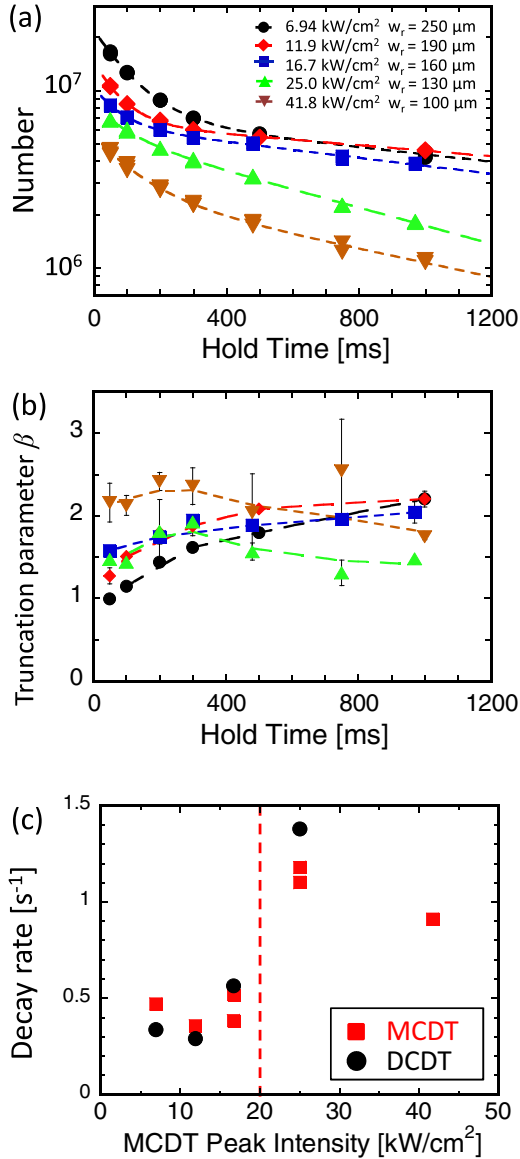


FIG. 3. Loss and heating in the compressed MCDT: (a) atom number, (b) temperature evolution, and (c) decay rate. In (a) and (b) the beam radii are 250  $\mu\text{m}$  (circles), 190  $\mu\text{m}$  (diamonds), 160  $\mu\text{m}$  (squares), 130  $\mu\text{m}$  (up triangles), and 100  $\mu\text{m}$  (down triangles). The peak intensity is for one beam. The decay curves are fits of the number data to a sum of two exponentials. Interpolated dashed lines in (b) are simply guides for the eye. In (c) the decay rate is the longer time constant of the fitted curves in (a). At  $\sim 20 \text{ kW}/\text{cm}^2$  (vertical dashed line), the rate suddenly changes by a factor of 2. The decay rates in the DCDT are also shown by solid circles as functions of the MCDT peak intensity. The definition of the decay rate is the same as that of the MCDT, except for the right end data, which is given by a single exponential fit.

The severe loss is caused by a process that was identified in previous studies [19,21]; two-photon transitions, which were induced by the two different frequencies of the multimode FL, pump the atoms to  $F = 2$  sublevels. Then hyperfine exchange collisions convert the internal energy into a kinetic energy that is large enough for the atoms to escape from the trap. We also observed a measurable increase in the population in  $F = 2$  at

a longer hold time (typically, over 500 ms, above  $I_{th}$ ). Since the pumping rate is the highest at the trap center, the coldest atoms are preferentially removed. This is considered to be a cause of the heating effect.

### C. Construction of a DCDT

As long as the intensity is below  $I_{th}$ , the MCDT can be compressed without severe loss and even evaporative cooling can be expected. However, even if the intensity was maintained below  $I_{th}$ , performing evaporation in the MCDT does not always promise to reach large condensates. Forced evaporation significantly reduces the collision rate. Furthermore, the loss due to the pumping can be avoided only by reducing the intensity.<sup>6</sup> These adverse effects prevent us from optimizing evaporation.

For faster and more efficient evaporation, we combine the MCDT with a smaller SCDT, forming a double compressible CDT. Modification of an original trap shape to change the PSD was first demonstrated by Pinkse *et al.* [23]. Soon after, the method to add a small “optical dimple” to an initial trap was developed by Stamper-Kurn *et al.* [24], where the dimple was turned on adiabatically and locally high PSD was obtained. Then it was shown by numerical simulations that the dimple geometry also affects the evaporation efficiency [25]. Jacob *et al.* utilized evaporation as an active tool to fill the dimple [13]. They combined a tight dimple trap with a CDT, both of which were already turned on at the time of loading from the MOT. As the gas is cooled by evaporation, the atoms gradually accumulate in the dimple, leading to large enhancements of both the spatial density and PSD of the whole of gas. For this “evaporative filling”, a high collision rate is a very important factor. Since more atoms are initially captured and smoothly squeezed in the double compressible CDT, the rate of filling is expected to increase.

Our strategy is as follows. First, we load numerous atoms in the enlarged DCDT. Next, by simultaneous compression, the SCDT is minimized while the beam intensity of the MCDT is kept lower than  $I_{th}$ . Immediately after the compression, we start forced evaporation by lowering only the MCDT power. Then we shut it off completely but continue evaporation in the SCDT. Along with this scenario, we set up the zoom-lens system as shown in Fig. 2. The minimum SCDT radius is 60  $\mu\text{m}$ , when the MCDT radius is 160  $\mu\text{m}$  and its intensity is  $16.7 \text{ kW}/\text{cm}^2 < I_{th}$ .

### D. Decay rate in a DCDT

The SCDT modifies the trap shape and changes the collision dynamics. To clarify the influence on  $I_{th}$ , we first consider a possible mechanism for the threshold behavior observed in the MCDT. We focus on the effect of the levitational field, which also modifies a trap. We neglect the hyperfine interaction and Zeeman energy at the location of the trap center, which are both position-independent energy offsets. The field gradient applied

<sup>6</sup>It has been demonstrated in a single-beam ODT that the two-photon transition can be controlled by applying a bias field and selecting a laser polarization. See Ref. [21].

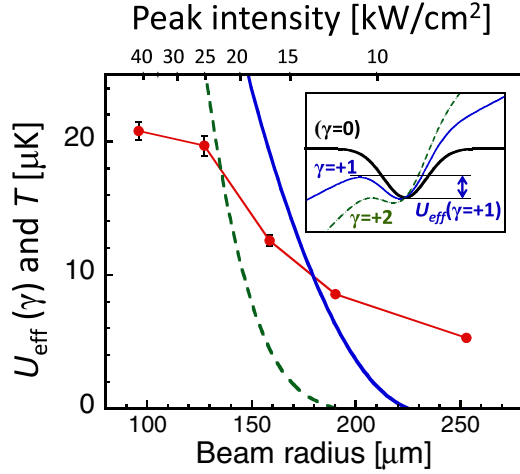


FIG. 4. Effective trap depths for  $\gamma = \pm 1$  states (blue solid line) and the  $\gamma = +2$  state (green dashed line) as functions of the radius. The measured temperatures are those at the 300-ms hold time and shown by red circles (with a line as a guide). The inset shows the potential curves of the MCDT along the  $z$  direction for  $w_r = 160 \mu\text{m}$  (the stage position equals 0). Here the  $\gamma = +1$  state is shown by the thin blue line, the  $\gamma = +2$  state by the thin dashed green line, and the  $\gamma = 0$  state by the thick black line. The position-independent energy offsets are subtracted.

satisfies  $g_F |\mu_B| \frac{dB}{dz} = mg$ ; here  $\mu_B$  is the Bohr magneton. Gravity is perfectly canceled out for the  $|11\rangle$  and  $|2-1\rangle$  states. The resulting gravitomagnetic potentials are sublevel dependent and equal to integer multiples of  $mgz$ . The total potentials are given by

$$U_\gamma(x, y, z) = -U_m \left[ \exp\left(-\frac{2x^2}{w_r^2} - \frac{2z^2}{w_z^2}\right) + \exp\left(-\frac{2y^2}{w_r^2} - \frac{2z^2}{w_z^2}\right) \right] + \gamma mgz. \quad (1)$$

Here the first term is the MCDT and  $w_r$  and  $w_z$  are the radial and vertical beam radii, respectively. The integer  $\gamma$  is 0 for  $|11\rangle$  and  $|2-1\rangle$  and for other sublevels  $\gamma$  takes the value  $-1$  ( $|2-2\rangle$ ),  $+1$  ( $|10\rangle$  and  $|20\rangle$ ),  $+2$  ( $|1-1\rangle$  and  $|21\rangle$ ), or  $+3$  ( $|22\rangle$ ).

For given beam radii, atoms can be trapped if  $U_m > U_{\min}(\gamma) = \frac{1}{4} \sqrt{e} |\gamma| mg w_z$  [11]. For very large radii, only  $\gamma = 0$  states have an energy minimum. When the radius becomes smaller, to satisfy  $U_m > U_{\min}(1)$ , another local minimum appears for  $\gamma = \pm 1$  states. This happens at  $w_r = 240 \mu\text{m}$ . Further compression rapidly increases the effective trap depth  $U_{\text{eff}}$ , as shown in Fig. 4. When  $U_{\text{eff}}(\gamma = \pm 1) \simeq k_B T$ , a large fraction of atoms in those states is trapped, providing many opportunities to collide with the atoms in  $\gamma = 0$  states and causing an additional loss. This starts at  $w_r = 180 \mu\text{m}$ . The intensity is  $13 \text{ kW/cm}^2$ , which is fairly close to  $I_{th}$ . The  $\gamma = 2$  state has similar characteristics:  $U_{\text{eff}}(\gamma = 2)$  starts to increase at a smaller radius and crosses the temperature curve at  $\sim 25 \text{ kW/cm}^2$ , which is very close to  $I_{th}$ .

If this scenario is correct, the loss may be aggravated in the compressed DCDT, where the sum of two beam intensities

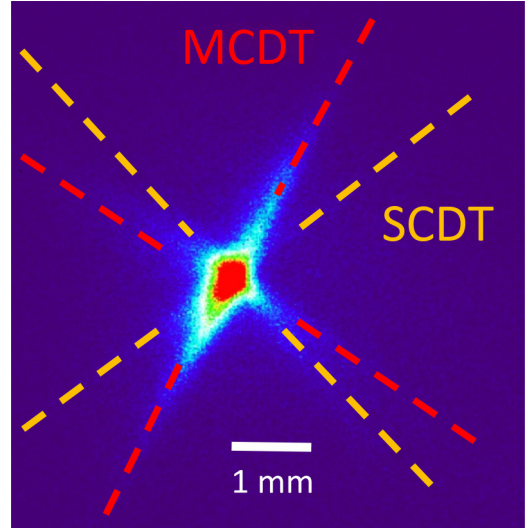


FIG. 5. *In situ* fluorescence image (top view) at the initial loading. The image is taken after 300 ms holding in the DCDT by using a high-intensity fluorescence probe [26]. Trapping beams are represented by dashed lines.

exceeds  $I_{th}$ . The DCDT can confine the atoms in all sublevels for  $w_r < 240 \mu\text{m}$ . In addition, the trapping frequency and the collision rate are much larger than those in the MCDT. However, we found the SCDT does not intensify the loss and the rates are virtually at the same levels as those in the MCDT, as shown in Fig. 3(c). This indicates that the loss rate is determined by the pumping rate to  $F = 2$ . Similar results were reported independently [21]. At the moment, it is reasonable to conclude that the sharp intensity dependence of the two-photon process simply looks like the threshold behavior. However, the pumping rate depends on individual experimental parameters such as the mode spacing, the beam intensity, and level structures of the atoms.<sup>7</sup> The mechanism that we presented is still worth considering for higher pumping rates.

In our case, the multimode FL intensity is the only concern. The DCDT described in Sec. III C ensures efficient evaporation. We observed that the truncation parameter increases from 3.5 to 5 during a 500-ms hold time.

## IV. BOSE-EINSTEIN CONDENSATE FORMATION IN A DCDT

### A. Initial loading into a DCDT

The atoms in the  $|11\rangle$  state are released from the 3D FORL and loaded into the enlarged DCDT. To determine the initial trap sizes, we measured the atom numbers after 300 ms at different stage positions. We consider these as the steady-state atom numbers. In an actual sequence, we start compression without any hold time. The largest number of  $2.3 \times 10^7$  was obtained when the radii of the MCDT and the SCDT were  $w_m = 440 \mu\text{m}$  and  $w_s = 210 \mu\text{m}$ , respectively. An *in situ* top view image is shown in Fig. 5. The DCDT

<sup>7</sup>For instance, spinless atoms do not suffer from the loss due to the pumping.

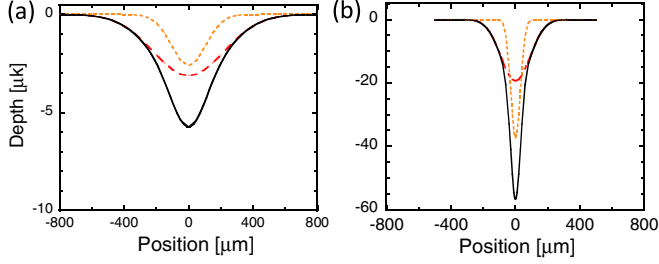


FIG. 6. Radial trapping potentials of a DCDT (black solid line), MCDT (red dashed line), and SCDT (orange dotted line). Both CDTs are assumed to be axially symmetric (a) at initial loading and (b) after compression.

potential is plotted in Fig. 6(a). The large MCDT recaptures a large number of atoms. In fact, the initial atom number in the MCDT alone is  $\sim 80\%$  of that in the DCDT. The SCDT is the driving force to pull down the atoms around the bottom.

### B. Compression of a DCDT

The scaling laws in Sec. III A are also valid for the DCDT for atoms around the trap center. The depth  $U_d$  is simply the sum of the two traps  $U_d = (U_m + U_s) \propto (\frac{P_m}{w_m^2} + \frac{P_s}{w_s^2})$ , while the trapping frequency is  $\omega_d = \sqrt{\omega_m^2 + \omega_s^2} \propto \sqrt{\frac{P_m}{w_m^4} + \frac{P_s}{w_s^4}}$ . In our case,  $U_s/U_d$  is 0.52 before and 0.64 after the compression. At the time of initial loading,  $\omega_m/2\pi$  and  $\omega_s/2\pi$  are 13 and 31 Hz, respectively. For a given number  $N$  and temperature  $T$ , the collision rate is  $\Gamma_{\text{col}} \propto N\omega^3/T$ . For the MCDT and DCDT,  $T$  at the loading is nearly the same and  $\Gamma_{\text{col}}$  in the DCDT is approximately 18 times greater than that in the MCDT. After the compression, the frequencies increase to 100 Hz for  $\omega_m/2\pi$  and 350 Hz for  $\omega_s/2\pi$ . The ratio  $\omega_s/\omega_d$  is  $\simeq 0.96$  and  $\omega_d/2\pi$  is virtually independent of  $P_m$ . Since  $\Gamma_{\text{col}}$  grows in proportion to  $\omega^2$  during an adiabatic process,  $\Gamma_{\text{col}}$  in the DCDT increases by over a factor of 2000 compared to that in the initial MCDT. In addition to the large increase in the collision rate, the DCDT enables us to rapidly decrease  $P_m$  without sacrificing  $\Gamma_{\text{col}}$ . The adiabatic compression is completed in one step by moving the stage by 9 mm in 370 ms. The corresponding trapping potential is shown in Fig. 6(b). Here  $1.1 \times 10^7$  atoms at 16  $\mu\text{K}$  are tightly confined. The PSD increases to 0.01 by unforced evaporation during the compression. The truncation parameter  $\beta_d \equiv U_d/k_B T = 3.9$  indicates that most atoms have already been around the DCDT center. The filling progresses further during subsequent forced evaporation. We will discuss the filling efficiency in Sec. V.

### C. Forced evaporation in a DCDT

Immediately after the compression, we start forced evaporation by reducing only the MCDT depth in three steps. We optimize the duration time to maximize the PSD at each step. The resulting PSD increases exponentially as shown in Fig. 7(a). During the first two steps,  $P_m$  is exponentially ramped down by 33% in 100 and 200 ms, respectively. The MCDT is then turned

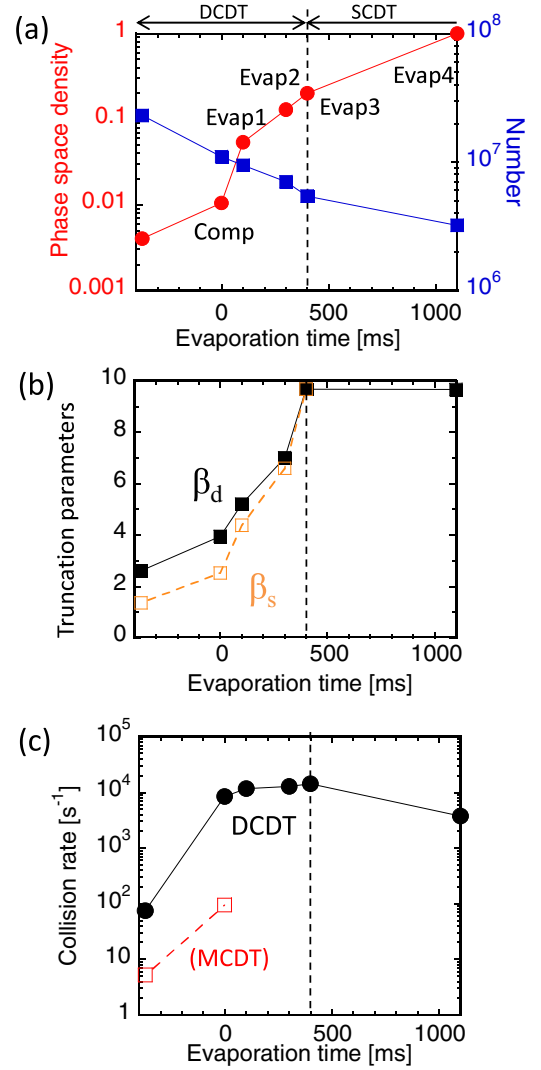


FIG. 7. (a) Progress of phase-space density: phase-space density (closed circles) and atom number (closed squares). The left end data are at the initial loading. (b) Time evolution of truncation parameters  $\beta_d = U_d/k_B T$  and  $\beta_s = U_s/k_B T$ . Here  $U_d = U_s$  after turning off the MCDT. (c) Calculated collision rates  $\Gamma_{\text{col}}$  in the DCDT (closed circles) and  $\Gamma_{\text{col}}$  in the MCDT at the initial loading and after the compression to 160  $\mu\text{m}$  are also shown (open squares). The collision rates are calculated as  $\Gamma_{\text{col}} = n v_{\text{th}} 8\pi a^2$ , where  $n$  is the peak density,  $v_{\text{th}} = \sqrt{3k_B T/m}$  is the thermal velocity, and  $a = 5.3$  nm is the scattering length of  $^{87}\text{Rb}$ .

off completely in 100 ms, leaving  $5 \times 10^6$  atoms in the SCDT. At this moment, the PSD  $\mathcal{D}$  reaches 0.2. Figure 7(b) shows that the truncation parameter increases progressively. This means the rethermalization is faster than the forced evaporation. It continues until  $\beta_d$  reaches  $\sim 10$  and the evaporation is stagnated [27]. While the atom number gradually decreases,  $\Gamma_{\text{col}}$  increases in each step as shown in Fig. 7(c). Although our estimation may not be very accurate, we consider that the evaporation is in the runaway regime. The cooling efficiencies  $\gamma_{\text{ev}} = -\Delta(\ln \mathcal{D})/\Delta(\ln N)$  maintain high values,  $\sim 3.8$  on average.

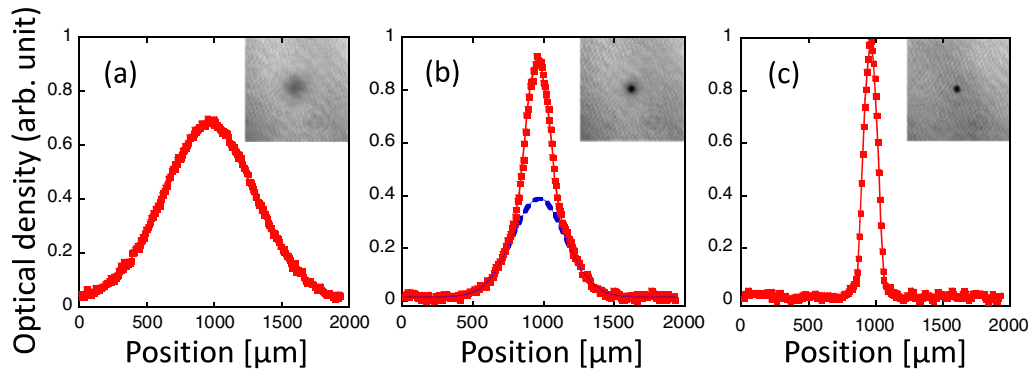


FIG. 8. Optical density profiles and absorption images at the last three stages of evaporation: (a) after the fourth evaporation, just before the BEC transition ( $N = 2.5 \times 10^6$  and  $T = 940$  nK); (b) after the fifth evaporation, bimodal density profile with 35% condensation ( $N = 1.8 \times 10^6$  and  $T = 390$  nK); and (c) after the final evaporation, almost pure condensation ( $N = 1.2 \times 10^6$ ). Images are taken after a 40-ms time of flight. A  $^{87}\text{Rb}$  BEC is created in the  $|Fm_F\rangle = |11\rangle$  state.

#### D. Forced evaporation in a SCDT

Before starting forced evaporation, the bias magnetic field is lowered to 4.5 G. After ramping down the SCDT power to 20%, the PSD increases to 1.0. This stage still has a very high collision rate, as indicated in Fig. 7(c), and  $\gamma_{ev}$  is also high,  $\sim 3.1$ . Another 20% ramp down in 900 ms makes a 35% BEC of  $1.8 \times 10^6$  atoms. Finally, a further 25% reduction, which is in total 1/100th of the initial  $P_s$ , yields more than 95% Bose condensed gas of  $1.2 \times 10^6$  atoms. This is the largest number among all-optical methods. The total time required is 3.6 s, including the compression. Figure 8 presents typical absorption images at the last three stages. The final transverse trapping frequency was measured to be 30 Hz and the chemical potential is 57 nK. The photon scattering rate is negligible,  $\sim 0.004$  Hz. The lifetime of the BEC was  $\sim 20$  s, limited by background pressure. We noticed that the laser power for the SCDT can be reduced without affecting the condensed atom number. Decreasing the power to  $\sim 50\%$  (0.9 W/beam) still yields a nearly pure BEC of  $1.0 \times 10^6$  atoms for almost the same duration.

### V. DISCUSSION

#### A. Efficient loading into a tight SCDT

Here we discuss the loading time and the efficiency for the tight SCDT by our double compression scheme. For comparison, let us suppose that a combined trap consists of two independent CDTs, both of which have fixed powers and sizes: 8.1 W and  $440 \mu\text{m}$  and 2 W and  $60 \mu\text{m}$ . These two traps are the initial MCDT and the minimum SCDT used in our experiments, but now act as a reservoir and a dimple, respectively. Since the gas released from the 3D FORL is density limited, the atom fraction directly entering into the dimple is tiny,  $\sim (60 \mu\text{m}/440 \mu\text{m})^3 \simeq 0.25\%$ . Thus, the most atoms would be captured in the reservoir at first. Assuming that the gas is in nearly equilibrium there, we consider the loading dynamics using a simple kinetic model presented in Ref. [28]. The model assumed that a dimple is very small, but very deep (depth much greater than temperature) with a small occupation and the gas is not in the hydrodynamic regime. The filling rate is determined by the atom flux entering

the dimple region and the scattering rate into the tightly bound states. The flux depends on both the trap geometry and the elastic collision rate in the reservoir. The scattering is caused by collisions between the entering atom and the already bounded one. Without evaporation, the loading time  $t_{\text{load}}$  is given by  $\sim 2t_{\text{coll}} \ln[\frac{N_f}{N_i} (\frac{l}{r_d})^3]$ , where  $N_i$  and  $N_f$  are the atom numbers in the reservoir and in the dimple, respectively [28]. Using the parameters in our experiments, i.e., the dimple size  $r_d = 60 \mu\text{m}$ , the reservoir size  $l = \sqrt{2k_B T/m\omega_m^2} \sim 250 \mu\text{m}$ , which is a thermal width in the MCDT, and the collision time  $t_{\text{coll}} = 1/\Gamma_{\text{col}} \simeq 200$  ms,  $t_{\text{load}}$  is estimated to be  $\sim 1$  s for only 10% filling.

Our compressible DCDT is in stark contrast to the fixed dimple trap. The atom fraction initially in the SCDT region is already significant,  $(210 \mu\text{m}/440 \mu\text{m})^3 \simeq 11\%$ . The gas is smoothly compressed and has very high collision rates, which hastens the loading process and, as a result, causes unforced evaporation. These processes start during the compression. The unforced and subsequent forced evaporations cause a continuous filling of the rest of the atoms dwelling outer parts in the MCDT into the SCDT. This can be seen in the plotted data of  $\beta_s = U_s/k_B T$  in Fig. 7(b), which starts from one-half of  $\beta_d$ , but soon takes nearly the same value after the first evaporation. We estimate the atom number in the SCDT  $N_s$  by assuming a noninteracting Boltzmann gas in a 3D harmonic potential with a depth of  $U_d$  and integrating the truncated energy distribution from 0 to  $U_s$ . After the compression,  $N_s$  is calculated to be  $\sim 60\%$  of the total number. Despite a gradual decrease of the total atom number,  $N_s$  increases by a factor of 1.5 during the first evaporation. In dimple traps or other hybrid traps [29], transferring atoms from a reservoir to a tighter region plays a crucial role. In our compressible DCDT, this transfer is carried out very quickly and efficiently.

#### B. Bose-Einstein condensate production in a 10-W SCDT

It is interesting to make a comparison between a DCDT and a high-power SCDT. By using a 10-W fiber amplifier with the same single-mode master laser, we created a SCDT in the same bow-tie geometry. First,  $1.5 \times 10^7$  atoms were loaded into the large-volume SCDT with an initial radius of  $400 \mu\text{m}$  ( $P_s = 6.4$  W/beam). The beam was then minimized to  $50 \mu\text{m}$

in two steps. Evaporation was performed in five steps, the first of which was done between the two compressions. After 4.6 s, we obtained a nearly pure BEC of  $1.5 \times 10^5$  atoms. In our DCDT, the minimum SCDT radius is slightly larger due to experimental limitations. Nevertheless, we could create an 8 times larger BEC in a shorter duration. This is due to a 1.5-fold improvement of the initial loading number and much higher collision rates realized in the DCDT.

## VI. CONCLUSION

We have described our all-optical approach to rapidly produce a large BEC of  $^{87}\text{Rb}$ . We have constructed a compressible DCDT consisting of a MCDT and a SCDT. Taking into account the threshold intensity observed for the MCDT, we design a compression scheme in which the SCDT is minimized when the beam intensity of the MCDT is just below  $I_{th}$ . The enlarged DCDT improves the initial atom number because of a high-power-based MCDT. By following adiabatic compression, nearly half of the initial atoms are loaded into the center part where the tight SCDT governs the collision dynamics. The filling into the SCDT is accelerated by evaporation that is close to the runaway regime until the PSD reaches 0.2. The transfer efficiency is as good as that of hybrid or dimple traps, but our loading is much faster.

Further evaporation in the SCDT yields a nearly pure BEC with  $1.2 \times 10^6$  atoms. This number is the largest among all-optical approaches. The average cooling efficiency is larger than 3. A 3.6-s total evaporation time shows that the production rate is also at the highest level. The results of our compressible DCDT have proven that this method improves former CDTs,

overcomes their known drawbacks, and circumvents intensity-dependent losses experienced by multimode FLs.

We have confirmed that the SCDT with less than 1 W can still create a BEC of  $10^5$ – $10^6$  atoms. A smaller beam size further relaxes the necessary power to the 100-mW level. One may construct this by using a TA or a high-power LD.

We suspect that the gas is in the hydrodynamic regime after being transferred to the SCDT. Three-body collisions may occur since the peak density is  $\sim 5 \times 10^{14}$  atoms/cm<sup>3</sup>. By having two or more steps of compression with evaporative cooling between them, one could control the atom density and the beam intensities more flexibly. A 100-W-class multimode FL could be applied. It would not be surprising if a BEC of more than  $10^7$  atoms could be realized in a few seconds. Our approach can also be applied to other atomic species.

## ACKNOWLEDGMENTS

We thank Masayuki Watanabe for helpful discussions and Hiroshi Kanemitsu, Syouta Sakatoku, Kazumasa Tanaka, Makoto Ogasawara, and Tsuyoki Sawa for their experimental assistance. We also thank Teruo Takahashi for his assistance in the construction of the experimental apparatus. This work was financially supported by the Japan Science and Technology Agency (PRESTO program), the Ministry of Education, Culture, Sports, Science and Technology of Japan (Grants-in-Aid for Scientific Research, Grants No. 20340106 and No. 24654131) and the Matsuo Foundation. K.Y. acknowledges a financial support from the Japan Society of Promotion of Science (Grant No. 24-984).

- 
- [1] W. Ketterle and N. J. van Druten, *Adv. At. Mol. Opt. Phys.* **37**, 181 (1996).
  - [2] J. Stenger, S. Inouye, D. M. Stamper-Kurn, H.-J. Miesner, A. P. Chikkatur, and W. Ketterle, *Nature (London)* **396**, 345 (1998).
  - [3] S. Inouye, M. R. Andrews, J. Stenger, H.-J. Miesner, D. M. Stamper-Kurn, and W. Ketterle, *Nature (London)* **392**, 151 (1998).
  - [4] S. Jochim, M. Bartenstein, A. Altmeyer, G. Hendl, S. Riedl, C. Chin, J. Hecker Denschlag, and R. Grimm, *Science* **302**, 2101 (2003).
  - [5] M. Greiner, C. A. Regal, and D. S. Jin, *Nature (London)* **426**, 537 (2003).
  - [6] C. S. Adams, H. J. Lee, N. Davidson, M. Kasevich, and S. Chu, *Phys. Rev. Lett.* **74**, 3577 (1995).
  - [7] S. J. M. Kuppens, K. L. Corwin, K. W. Miller, T. E. Chupp, and C. E. Wieman, *Phys. Rev. A* **62**, 013406 (2000).
  - [8] M. D. Barrett, J. A. Sauer, and M. S. Chapman, *Phys. Rev. Lett.* **87**, 010404 (2001).
  - [9] S. R. Granade, M. E. Gehm, K. M. O'Hara, and J. E. Thomas, *Phys. Rev. Lett.* **88**, 120405 (2002).
  - [10] K. M. O'Hara, M. E. Gehm, S. R. Granade, and J. E. Thomas, *Phys. Rev. A* **64**, 051403(R) (2001).
  - [11] C.-L. Hung, X. Zhang, N. Gemelke, and C. Chin, *Phys. Rev. A* **78**, 011604(R) (2008).
  - [12] T. Weber, J. Herbig, M. Mark, H.-C. Nägerl, and R. Grimm, *Science* **299**, 232 (2003).
  - [13] D. Jacob, E. Mimoun, L. De Sarlo, M. Weitz, J. Dalibard, and F. Gerbier, *New J. Phys.* **13**, 065022 (2011).
  - [14] J.-F. Clément, J.-P. Brantut, M. Robert-de-Saint-Vincent, R. A. Nyman, A. Aspect, T. Bourdel, and P. Bouyer, *Phys. Rev. A* **79**, 061406(R) (2009).
  - [15] M.-O. Mewes, M. R. Andrews, N. J. van Druten, D. M. Kurn, D. S. Durfee, and W. Ketterle, *Phys. Rev. Lett.* **77**, 416 (1996).
  - [16] D. J. Han, M. T. DePue, and D. S. Weiss, *Phys. Rev. A* **63**, 023405 (2001).
  - [17] T. Kinoshita, T. Wenger, and D. S. Weiss, *Phys. Rev. A* **71**, 011602(R) (2005).
  - [18] R. Roy, A. Green, R. Bowler, and S. Gupta, *Phys. Rev. A* **93**, 043403 (2016).
  - [19] T. Lauber, J. Küber, O. Wille, and G. Birkl, *Phys. Rev. A* **84**, 043641 (2011).
  - [20] S. Kumar, S. Hirai, Y. Suzuki, M. Kachi, M. Sadgrove, and K. Nakagawa, *J. Phys. Soc. Jpn.* **81**, 084004 (2012).
  - [21] W. Hung, P. Huang, F.-C. Wu, M. Bruvelis, H.-Y. Xiao, A. Ekers, and I. A. Yu, *J. Opt. Soc. Am. B* **32**, B32 (2015).
  - [22] S. L. Winoto, M. T. DePue, N. E. Bramall, and D. S. Weiss, *Phys. Rev. A* **59**, R19(R) (1999).
  - [23] P. W. H. Pinkse, A. Mosk, M. Weidemüller, M. W. Reynolds, T. W. Hijmans, and J. T. M. Walraven, *Phys. Rev. Lett.* **78**, 990 (1997).

- [24] D. M. Stamper-Kurn, H.-J. Miesner, A. P. Chikkatur, S. Inouye, J. Stenger, and W. Ketterle, *Phys. Rev. Lett.* **81**, 2194 (1998).
- [25] Z.-Y. Ma, C. J. Foot, and S. L. Cornish, *J. Phys. B* **37**, 3187 (2004).
- [26] M. T. DePue, S. L. Winoto, D. J. Han, and D. S. Weiss, *Opt. Commun.* **180**, 73 (2000).
- [27] O. J. Luiten, M. W. Reynolds, and J. T. M. Walraven, *Phys. Rev. A* **53**, 381 (1996).
- [28] D. Comparat, A. Fioretti, G. Stern, E. Dimova, B. Laburthe Tolra, and P. Pillet, *Phys. Rev. A* **73**, 043410 (2006).
- [29] Y.-J. Lin, A. R. Perry, R. L. Compton, I. B. Spielman, and J. V. Porto, *Phys. Rev. A* **79**, 063631 (2009).